Resistance to Avapritinib in PDGFRA-Driven GIST Is Caused by Secondary Mutations in the PDGFRA Kinase Domain

Susanne Grunewald[1,2], Lillian R. Klug[3], Thomas Mühlenberg[1,2], Jonas Lategahn[4,5], Johanna Falkenhorst[1,2], Ajia Town[3], Christiane Ehrt[4,5], Eva Wardelmann[6], Wolfgang Hartmann[6], Hans-Ulrich Schildhaus[7], Juergen Treckmann[8], Jonathan A. Fletcher[9], Sascha Jung[4], Paul Czodrowski[4], Stephen Miller[10], Oleg Schmidt-Kittler[10], Daniel Rauh[4,5], Michael C. Heinrich[3], and Sebastian Bauer[1,2]

ABSTRACT Gastrointestinal stromal tumors (GIST) harboring activating mutations of *PDGFRA* respond to imatinib, with the notable exception of the most common mutation, D842V. Avapritinib is a novel, potent KIT/PDGFRA inhibitor with substantial clinical activity in patients with the D842V genotype. To date, only a minority of *PDGFRA*-mutant patients treated with avapritinib have developed secondary resistance. Tumor and plasma biopsies in 6 of 7 patients with *PDGFRA* primary mutations who progressed on avapritinib or imatinib had secondary resistance mutations within *PDGFRA* exons 13, 14, and 15 that interfere with avapritinib binding. Secondary *PDGFRA* mutations causing V658A, N659K, Y676C, and G680R substitutions were found in 2 or more patients each, representing recurrent mechanisms of PDGFRA GIST drug resistance. Notably, most PDGFRA-mutant GISTs refractory to avapritinib remain dependent on the PDGFRA oncogenic signal. Inhibitors that target PDGFRA protein stability or inhibition of PDGFRA-dependent signaling pathways may overcome avapritinib resistance.

SIGNIFICANCE: Here, we provide the first description of avapritinib resistance mechanisms in PDGFRA-mutant GIST.

INTRODUCTION

Gastrointestinal stromal tumors (GIST) are the most common sarcoma subtype and are thought to arise from oncogenic transformation of interstitial cells of Cajal (ICC) precursors found in the smooth muscle wall of the stomach and intestines (1, 2). Mutations of *KIT* or *PDGFRA*, both of which are intrinsically expressed at high levels during ICC differentiation, lead to constitutive activation of these kinases (3). Activating mutations in either *KIT* or *PDGFRA* are found in most GISTs and appear to function as the initiating oncogenic events (3–5).

[1]Department of Medical Oncology, Sarcoma Center, West German Cancer Center, University Duisburg-Essen, Medical School, Essen, Germany. [2]DKTK partner site Essen, German Cancer Consortium (DKTK), Heidelberg, Germany. [3]Portland VA Health Care System, Portland, Oregon; Knight Cancer Institute, Oregon Health and Science University, Portland, Oregon; and Division of Hematology and Medical Oncology, Oregon Health and Science University, Portland, Oregon. [4]Faculty of Chemistry and Chemical Biology, TU Dortmund University, Dortmund, Germany. [5]Drug Discovery Hub Dortmund (DDHD) am Zentrum für Integrierte Wirkstoffforschung (ZIW), Dortmund, Germany. [6]Gerhard-Domagk-Institute of Pathology, University of Münster Medical Center, Münster, Germany. [7]Institute of Pathology, University Medical Center Essen, Essen, Germany. [8]Department of Visceral Surgery, Sarcoma Center, West German Cancer Center, University Duisburg-Essen, Medical School, Essen, Germany. [9]Department of Pathology, Brigham and Women's Hospital, Boston, Massachusetts. [10]Blueprint Medicines, Cambridge, Massachusetts.

Note: Supplementary data for this article are available at Cancer Discovery Online (http://cancerdiscovery.aacrjournals.org/).

S. Grunewald, L.R. Klug, and T. Mühlenberg contributed equally to this work. M.C. Heinrich and S. Bauer contributed equally to this work.

Corresponding Author: Sebastian Bauer, Department of Medical Oncology, West German Cancer Center, Sarcoma Center, University Duisburg-Essen, Essen, Germany; DKTK partner site Essen and German Cancer Consortium (DKTK), West German Cancer Center, University Hospital Essen, Hufeland-str. 55, Essen 45122, Germany. Phone: 49-201-723-2112; Fax: 49-201-723-3112; E-mail: sebastian.bauer@uk-essen.de

PDGFRA and *KIT* map to adjacent genomic loci on Ch4q12, and their protein structures are highly homologous. Both belong to the type III receptor tyrosine kinase family, which is characterized by an extracellular ligand binding domain, a transmembrane domain, and an intracellular catalytic domain (6). Effective biochemical inhibition of mutant forms of KIT and PDGFRA strongly correlates with clinical response in patients with GIST with metastatic disease (7). Primary, activating KIT mutations are most commonly found in the intracellular juxtamembrane domain (JM; exon 11) or in the extracellular dimerization domain (exon 9), with only rare cases involving the ATP-binding domain (exon 13) or activation loop (exon 17; ref. 3). In contrast, in *PDGFRA*-mutant GIST, the majority of primary oncogenic mutations are found in the activation loop (AL; exon 18) and commonly involve codon 842, and more rarely affect the JM (exon 12) or ATP-binding domain (exon 14). GISTs that do not exhibit mutations in either KIT or PDGFRA often display alternative mechanisms (e.g., mutations of NF1, PI3K, BRAF, KRAS, FGFR, and NTRK3) to constitutively activate the same downstream pathways that are typically activated by oncogenic KIT or PDGFRA (8, 9).

The spectrum of primary *KIT* or *PDGFRA* mutations found in GIST is broad, involving point mutations, deletions, and insertions–deletions, and the various oncogenic mutants exhibit different enzymatic, cellular, and protein dynamic properties (7, 10). Not surprisingly, these mutations are also predictive for the response to KIT and PDGFRA inhibitors (7, 11, 12). As seen in other kinase-driven cancers treated with kinase inhibitors, KIT-mutant GISTs that progress after response to KIT inhibitors very frequently contain secondary mutations within the ATP-binding domain (exons 13–14) or the AL (exons 17–18) of KIT, as these types of mutations disrupt drug binding (11, 12). In contrast, little is known about mechanisms of resistance in *PDGFRA*-mutant GIST—except for primary or secondary *PDGFRA*[D842V] mutations. This particular mutation is resistant to the initially approved kinase inhibitors for GIST, and therefore patients with advanced *PDGFRA*[D842V]-mutant

GIST have historically had a poor prognosis (13, 14). Recently, avapritinib (BLU-285), a novel, fourth-generation type I kinase inhibitor specifically designed to inhibit PDGFRA^{D842V}, has been shown to be highly potent against this mutation, with biochemical IC$_{50}$ values in the low nanomolar range (15). Clinical data suggest efficacy of avapritinib for D842V-mutant GIST that parallels or even exceeds the activity of imatinib in *KIT* exon 11–mutant GIST (15, 16). Notably, in January 2020, avapritinib was approved by the FDA for first-line treatment of GIST with *PDGFRA* mutations in exon 18. Despite the profound clinical responses of patients with *PDGFRA*-mutant GIST, some patients with *PDGFRA* mutations treated within the recent NAVIGATOR trial [NCT02508532; A Phase I Study of BLU-285 in Patients with Gastrointestinal Stromal Tumors (GIST) and Other Relapsed and Refractory Solid Tumors] have progressed following an initial response to avapritinib. Here we describe, for the first time, the mechanisms of resistance to avapritinib in *PDGFRA*-mutant GIST based on 7 patient cases and investigate salvage therapies to overcome resistance *in vitro*.

RESULTS

Clinical Evidence and Significance of Resistance

The NAVIGATOR trial is a two-part, open-label, dose-escalation/expansion study that investigated avapritinib in patients with *PDGFRA*^{D842V}-mutant GIST or GIST with other mutations that had progressed on imatinib or post-imatinib tyrosine kinase inhibitors (16). In total, 43 patients with *PDGFRA* exon 18–mutant GIST have been treated within the trial at the 300-mg and 400-mg dose levels, of whom 84% had an objective radiologic response, as assessed by mRECIST1.1 criteria. As of November 2019, 11 patients, representing 26% of this cohort, have experienced true on-treatment progression. Given the lack of therapeutic alternatives, most patients continued treatment beyond progression, but some underwent routine diagnostic biopsies or therapeutic resections of progressing lesions. Median overall survival from time after documented progression was only 5.2 months and a mere 0.5 months from the last dose of avapritinib (Supplementary Fig. S1A). We sought to identify mechanisms of resistance in these patients.

Circulating tumor DNA (ctDNA) is potentially useful in investigating resistance to kinase inhibitors, as plasma sequencing potentially offers a broader picture of clonal heterogeneity than needle biopsy of a single lesion. Recently, several clinical studies investigated ctDNA levels in patients with *KIT*-mutant GIST, with most patients having a low abundance of ctDNA compared with many common cancers (17). As an exploratory study within the

NAVIGATOR trial, we investigated the usefulness of plasma sequencing for detection of mutational information from *PDGFRA*-mutant GIST (18). ctDNA was isolated from 60 patients at baseline and analyzed by either BEAMing (beads, emulsion, amplification, magnetics—digital PCR) or panel next-generation sequencing (NGS). The genotype of the primary *PDGFRA* mutation was known for all patients based on local tumor biopsy sequencing results. In total, mutant ctDNA was detected in 63% (38/60) of patients (Fig. 1A). Using BEAMing technology, the detection rate of the primary mutation was 64% (14/22) compared with 53% (20/38) for NGS. In patients with detectable ctDNA, the mean allelic frequency (MAF) of the primary mutations was 3.49% (Fig. 1A). In plasma samples that were analyzed by panel NGS, only the primary *PDGFRA* mutation was detected. We then calculated the sum of all target lesions of each patient and correlated tumor load with levels of mutant plasma DNA. In patients with detectable ctDNA, the median sum of target lesions (as per mRECIST version 1.1) was 18.2 cm, compared with 7.5 cm for those without detectable ctDNA. This suggests that ctDNA detection might be influenced, and potentially limited, by individual patient tumor burden.

Among the 11 patients harboring *PDGFRA* exon 18 mutations progressing on avapritinib, pre- and post-progression plasma and/or tumor samples were available for four patients. Patients 1, 2, and 3 harbored typical D842V point mutations, whereas patient 4 had an in-frame deletion in exon 18 (I843_D846del, also referred to as delDIMH842-845 in the literature). These patients had received avapritinib at initial doses of 60 to 300 mg that resulted in tumor shrinkage by mRECIST version 1.1 or reduction of density of metastatic lesions, with maximum responses observed after 6 to 8 months of treatment and concordant disappearance of mutant ctDNA from plasma (Fig. 1B). Evidence of progression was found by radiographic imaging after 8.5 to 17 months of therapy, albeit the first progression in patient 4 was detected during a treatment break to manage side effects (Fig. 1B). Mutant ctDNA became detectable again in the plasma at the time of clinical progression in all four patients. All four patients underwent diagnostic biopsies and/or surgical removal of tumors post-progression.

Mutational analysis was performed on post-progression plasma and/or tumor samples to identify mechanisms of resistance. Although pretreatment samples of all patients included in this analysis exclusively showed primary *PDGFRA* mutations, post-progression samples revealed various mechanisms of resistance. Patients 1, 3, and 4 had several novel *PDGFRA* mutations detected using both plasma and tumor sequencing. These novel mutations were found in

Figure 1. Correlation of tumor size and treatment with the detection of mutant DNA in plasma. **A,** Plasma sequencing of 60 patients treated within the NAVIGATOR trial at baseline using either BEAMing or NGS sequencing. Bar graphs show allelic frequency of *PDGFRA* mutations in ctDNA. Detection rate of mutant DNA depending on the detection method; X = method used. For non-D842V row 1 = I843_D846del; 2 = N659K; 3 = DI842_843V. **B,** CT images of avapritinib-treated patients with *PDGFRA*-mutant GIST at baseline, at the time of best response, and at time of progression. Total tumor diameter over treatment time and MAF of *PDGFRA* primary mutations as measured by BEAMing (patients 1 and 2) or PGDx PlasmaSelect64 assay (patients 3 and 4) is plotted below (※surgery, lesion classification using mRECIST1.1 criteria). Note re patient 3: The deep pelvic lesion depicted at baseline was located closer to the pelvic inlet in the follow-up scan (BR) and was later surgically resected. BR, best response; P, progressive disease.

A

B
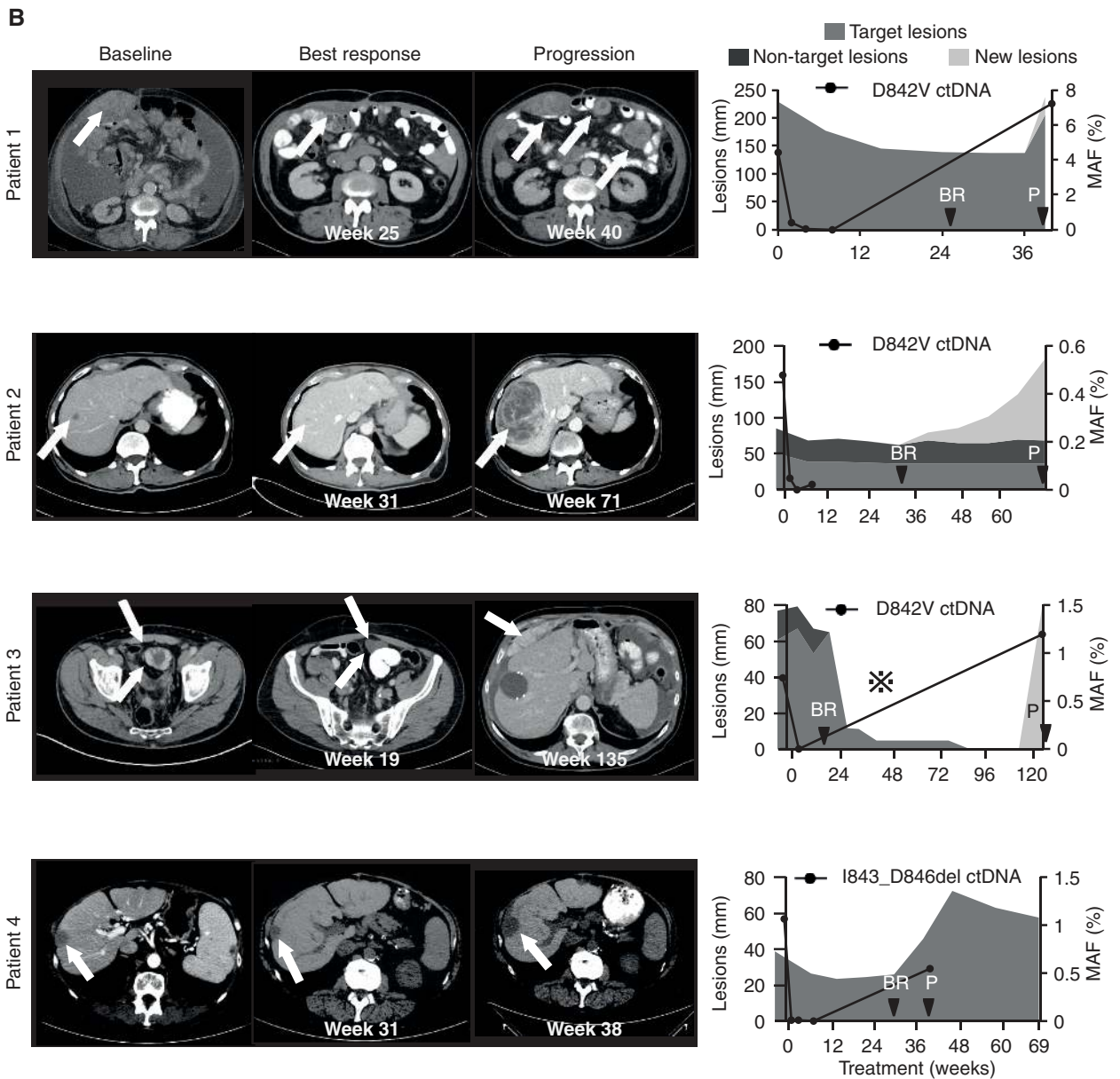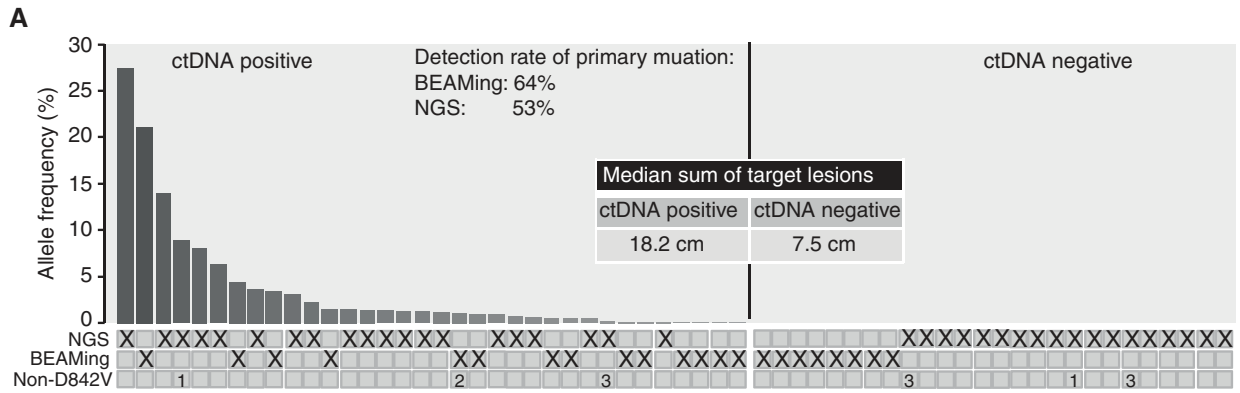
exons 13, 14, and 15, involving codons 598, 652, 658, 674, 676, and 680 (Table 1). Interestingly, in the case of patient 1, one lesion included compound (intra-allelic) secondary mutations G652E and V658A, whereas other lesions in this patient showed only V658A. Exome sequencing of the resistant tumor in patient 1 revealed this mutation to be homozygous (Supplementary Table S1), confirming that most, if not all, mutations must be in *cis*. In addition, mutations of codons 658 and 680 were found independently in other patients whose GIST had different primary mutations, suggesting that codon 658 and 680 mutations represent a recurrent cause of resistance. To exclude clonal hematopoiesis as a source for mutant *PDGFRA* in plasma, we analyzed all plasma samples from the NAVIGATOR, VOYAGER, and the ARROW studies for the presence of *PDGFRA* mutations. Notably, no mutations of *PDGFRA* were found in non–*PDGFRA*-mutant patients from the VOYAGER (GIST; *n* = 417) or ARROW (non–small cell lung cancer; *n* = 398) studies (Supplementary Table S2).

Whole-exome sequencing of pre- and post-progression tumor samples was performed in patient 1 to gain a more complete view of mutations that could be contributing to avapritinib resistance, but only *PDGFRA* mutations were identified as relevant genomic findings (Supplementary Table S1).

Only one patient (patient 2) lacked secondary *PDGFRA* mutations post-progression. Plasma sequencing identified mutations in genes that could constitutively activate the PI3K pathway and/or the MAPK pathway (*TSC1* and *NF1*, respectively). In the context of *KIT*-mutant GIST, these mutations have been shown to supplant KIT as drivers (19) and confer resistance to KIT inhibitors *in vitro* (18). For avapritinib-naïve *PDGFRA*-mutant GIST, mutations involving these pathways have not been reported (14). These events are likely underreported in routine pathology reports but may become more relevant with the development of more potent KIT inhibitors. In the present study, both genomic events were found in post-progression tumor or plasma samples in only a single patient; further studies are needed to determine the clinical relevance of these mutations in the context of *PDGFRA*-mutant GIST. As baseline tumor material was not available, it is unclear if these mutations were preexisting or emerged during avapritinib treatment (19).

Little is known about mechanisms of imatinib resistance in patients with primary, imatinib-sensitive (non-D842V) *PDGFRA* mutations. We hypothesized that mutations that confer resistance to imatinib might also confer cross-resistance to avapritinib. This information could provide clinically relevant information to guide the management of patients with *PDGFRA*-mutant GIST. In addition to patients treated within the NAVIGATOR trial, we further searched institutional databases for patients having secondary *PDGFRA* mutations that could represent potential mechanisms for imatinib resistance. We identified one patient (patient 5) with a primary *PDGFRA* exon 14 mutation, N659K, who had previously progressed on imatinib, sunitinib, and regorafenib (Table 1). Post-progression samples from this patient's tumors, taken following progression on imatinib and sunitinib, harbored a second mutation resulting in a T674R substitution affecting the gatekeeper residue (20). Through participation in a compassionate-use program, patient 5 was treated with avapritinib at a dose of 200 mg

daily but exhibited rapid progression (Supplementary Fig. S1B). This suggests that mutations at the gatekeeper residue may also confer resistance to avapritinib. Two other patients with imatinib-sensitive, *PDGFRA* exon 18 primary mutations were both found to have the G680R secondary mutation in the plasma with an allelic frequency of 8.8% (patient 6) and 0.8% (patient 7). Patient 7 received avapritinib afterward within the VOYAGER trial and attained a partial response as best response but had a relatively short progression-free survival of 11.1 months compared with the median progression-free survival of patients treated in the NAVIGATOR study.

Validation of Secondary Resistance Mutations *In Vitro*

To validate the putative resistance mutations found in clinical samples, we created cell line models to assess the effects of imatinib and avapritinib on PDGFRA tyrosine phosphorylation. First, we created Ba/F3 cell lines driven by the primary mutations observed in patients from the NAVIGATOR trial (PDGFRA^{D842V} or PDGFRA$^{I843-D846del}$). As expected, the primary mutation seen in patients 1 to 3, PDGFRA^{D842V}, was highly sensitive to avapritinib (IC$_{50}$ = 4 nmol/L), but resistant to imatinib (Fig. 2A–I; Supplementary Figs. S2A–S2M and S3A–S3I). We then investigated the effect of the secondary mutations seen in patient 1 on sensitivity to avapritinib and observed different levels of avapritinib resistance with each mutation. The mutant kinase with an exon 13 secondary mutation, PDGFRA$^{D842V/V598F}$, conferred significant resistance to avapritinib (IC$_{50}$ = 464 nmol/L). The double mutant PDGFRA$^{D842V/V658A}$ exhibited a greater than 5-fold higher IC$_{50}$ value for inhibition of PDGFRA phosphorylation (26 nmol/L) compared with PDGFRA^{D842V} (Fig. 2; Supplementary Fig. S2). The addition of a third mutation, resulting in PDGFRA$^{D842V/V658A/G652E}$, further increased resistance with a more than 40-fold higher IC$_{50}$ value (170 nmol/L) compared with the D842V-only mutant. The addition of G680R to D842V (PDGFRA$^{D842V/G680R}$) was associated with the highest level of resistance to avapritinib with an IC$_{50}$ value for PDGFRA phosphorylation above 1,000 nmol/L. Despite being identified at a low allelic fraction in the plasma of patient 1, we confirmed that PDGFRA$^{D842V/QGPins}$ conferred biochemical resistance to avapritinib (IC$_{50}$ = 102 nmol/L). In addition, the Y676C secondary mutation identified in patient 3 increased the IC$_{50}$ value of avapritinib by more than 100-fold over PDGFRA^{D842V} alone (IC$_{50}$ = 484 nmol/L).

We then used a Ba/F3 model driven by PDGFRA$^{I843-D846del}$ to model the mutations seen in patient 4. This primary mutation was sensitive to avapritinib (IC$_{50}$ = 2 nmol/L), as well as imatinib, as expected (Fig. 2; Supplementary Figs. S2 and S3). Of the three secondary mutations found in patient 4, two (V658A and G680R) were also seen in patient 1 in the context of the PDGFRA^{D842V} primary mutation. Similar to what was seen in patient 1 (PDGFRA^{D842V}), these mutations conferred resistance to avapritinib in the context of PDGFRA$^{I843-D846del}$, but to different extents: PDGFRA$^{I843-D846del/V658A}$ had an IC$_{50}$ value 24-fold higher than the primary PDGFRA$^{I843-D846del}$ alone (48 nmol/L), whereas PDGFRA$^{I843-D846del/G680R}$ was highly resistant (>1,000 nmol/L). The exon 14 mutation N659K was seen as a secondary mutation in conjunction with PDGFRA$^{I843-D846del}$

Table 1. Oncogenic mutations found in patients with *PDGFRA*-mutant GIST progressing on kinase-inhibitory treatment

	Patient	Treatment stage	PDGFRA mutation	Exon	Sample origin	Allelic fraction	Method
NAVIGATOR trial	1	Pre-ava	**D842V**	18	Tumor	89%	A
					Plasma	4.4%	B
		Post-ava	**D842V**	18	Tumor	91%	A
			G652E[a]	14		89.8%	
			V658A[a]	14		90.3%	
			D842V	18	Plasma	12.1%	C
			V598F	13		1.1%	
			G652E	14		7.1%	
			V658A	14		1.2%	
			G680R[b]	15		3.3%	
			G680R[c]	15		0.06%	
			V658A	14		1.5%	D
			G680R	15		9.1%	
			QGPins	14		0.2%	
	2	Pre-ava	**D842V**	18	Tumor	n.k.	E
					Plasma	0.48%	B
		Post-ava	**D842V**	18	Tumor[d]	88.2%	A
			D842V	18	Plasma[e]	4.1%	D
	3	Pre-ava	**D842V**	18	Tumor	40.1%	F
					Plasma	0.74%	C
		Post-ava	**D842V**	18	Tumor[f]	39.3%	G
			D842V	18	Tumor	40.9%	G
			D842V	18	Plasma	1.2%	D
			Y676C	15		0.9%	
	4	Pre-ava	**I843_D846del**	18	Tumor	50%[f]	E
					Plasma	1.05%	C
		Post-ava	**I843_D846del**	18	Tumor #1	96%	H
			G680R	15		37%	
			I843_D846del	18	Tumor #2	76%	H
			V658A	14		14%	
			G680R	15	Plasma	0.8%	H
			N659K	14		0.9%	
Other	5	Pre-im	**N659K**	14	Tumor	n.k.	B
		Post-im	**N659K**	14	Tumor	34%	G
			T674R	15		33%	
			N659K	14	Plasma	2.2%	D
			T674R	15		1.4%	
	6	Pre-im/su	unknown				-
		Post-im/su	D842_D846delinsE	18	Plasma	16.3%	G
			G680R	15		8.8%	
	7	Pre-im/su/sora	unknown				-
		Post-im/su/sora	D842_D846delinsV	18	Plasma	11.1%	G
			G680R	15		0.8%	
			Y676C	15		0.2%	

NOTE: Pathogenic mutations found in pre- and post-progression tumor and circulating plasma DNA in patients treated in the NAVIGATOR trial (patients 1–4; ava, avapritinib) as well as genomic findings in three patients with non-D842V GIST pretreated with imatinib (im) and sunitinib (su; patients 5 and 6) and with imatinib, sunitinib, and sorafenib (sora; patient 7), in a routine clinical setting. Primary mutations are boldface. In patients 6 and 7, baseline sequencing was not available but D842V_D846delins are previously described primary mutations.
Methods used for tumor sequencing:
A: Whole-exome sequencing (Genewiz); B: BEAMing; C: NGS Panel Sequencing (PGDx Plasma Select64); D: NGS Panel Sequencing (Guardant 360); E: Sanger sequencing; F: NGS Panel Sequencing (PGDx Cancer Select 125); G: NGS Panel Sequencing (Qiagen customized cancer panel CCP V3.0, University Hospital Essen, Germany); H: OHSU NGS panel.
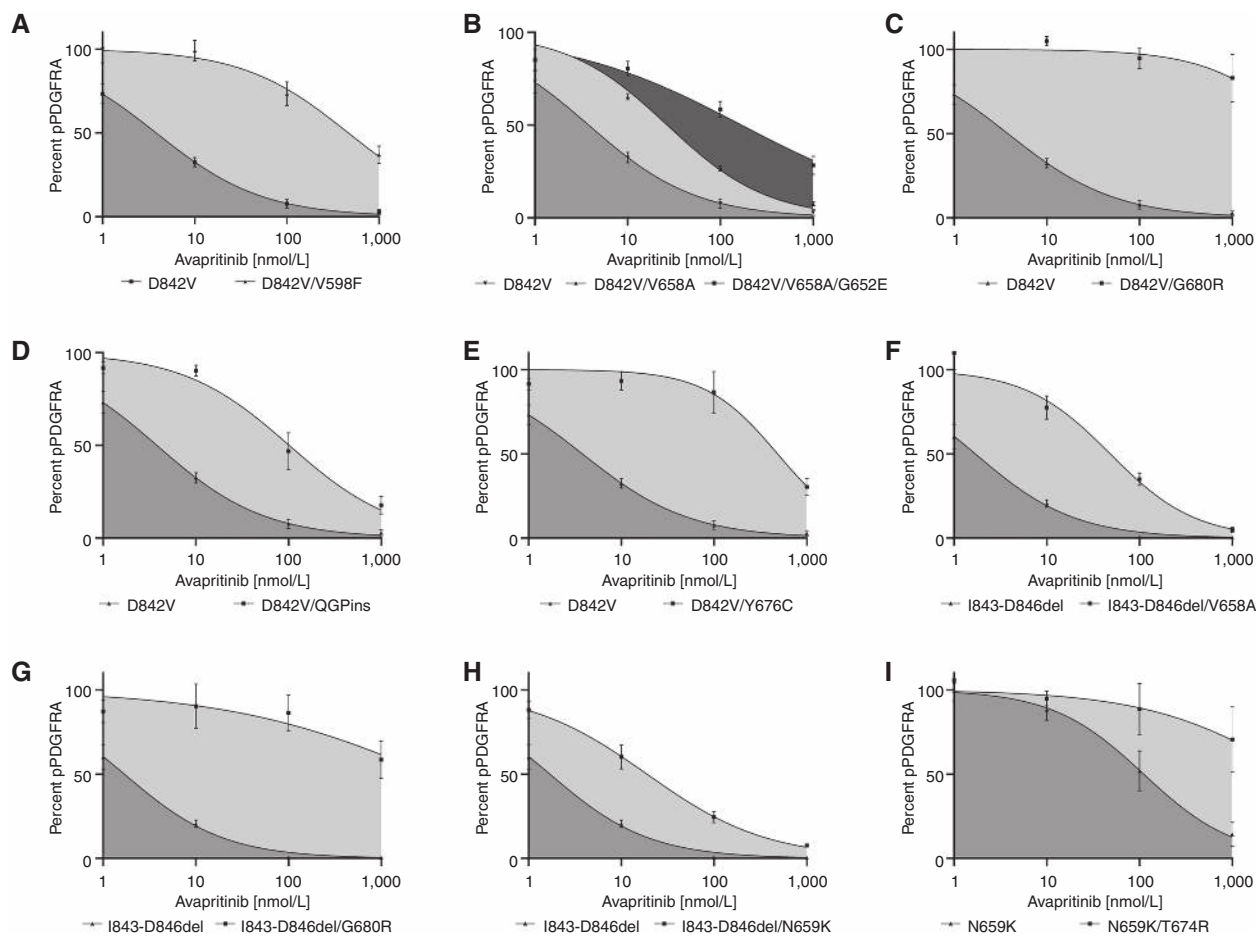[a]Mutations found on the same allele.
[b]2038G>A.
[c]2038G>C.
[d]Additional downstream mutation found: TSC1 deletion (AF 10.9%) and
[e]NF1 F2156V (AF 0.1%).
[f]Progression during treatment break.

Figure 2. *PDGFRA*-mutant models display varying levels of avapritinib resistance. **A–I,** Immunoblot quantification of the effect of avapritinib on phosphorylation of PDGFRA mutants observed in patient 1 (**A–D**) or patient 4 (**F–H**) modeled in Ba/F3 cell lines, and PDGFRA mutants observed in imatinib-resistant patients 3 (**E**) and 5 (**I**). Mutations involving N659K were not able to support IL3-independent Ba/F3 growth; these mutants were modeled using a transfection system in CHO cells. Data points represent average of at least 3 independent experiments with SEM shown. Nonlinear regression curve shown for each data set was used to calculate IC_{50} (GraphPad Prism).

in patient 4. When tested in our model, $PDGFRA^{I843-D846del/N659K}$ increased the IC_{50} value for avapritinib 15-fold (30 nmol/L). Of the secondary mutations seen in patient 4, all also conferred resistance to imatinib compared with $PDGFRA^{I843-D846del}$ alone (Supplementary Fig. S3). Of note, in the context of the imatinib-sensitive $PDGFRA^{I843-D846del}$ primary mutation, cells with additional G680R remained moderately sensitive to imatinib ($IC_{50} = 46$ nmol/L), whereas $PDGFRA^{I843-D846del/V658A}$ and $PDGFRA^{I843-D846del/N659K}$ conferred resistance to imatinib ($IC_{50} > 200$ nmol/L; Supplementary Fig. S3).

In addition, we modeled both the primary mutation ($PDGFRA^{N659K}$) and secondary mutation ($PDGFRA^{N659K/T674R}$) seen in patient 5, who had previously progressed on imatinib and sunitinib before tissue analysis and rapidly progressed on avapritinib afterward. We found that $PDGFRA^{N659K}$ was resistant to imatinib ($IC_{50} = 253$ nmol/L) and also to avapritinib ($IC_{50} = 91$ nmol/L) compared with $PDGFRA^{D842V}$ (Fig. 2; Supplementary Figs. S2 and S3). $PDGFRA^{N659K/T674R}$ conferred strong resistance to both avapritinib ($IC_{50} > 1,000$ nmol/L) and imatinib ($IC_{50} > 1,000$ nmol/L), suggesting the

gatekeeper residue also plays an important role in avapritinib binding.

PDGFRA-Driven GIST Models Recapitulate Clinical Resistance

Prior to this study, no *PDGFRA*-mutant human GIST cell lines were available. We were able to derive a GIST cell line from a post-progression tumor sample from patient 1, which we used to investigate avapritinib resistance in this patient (Fig. 3A). This primary *PDGFRA*-mutated cell line (Trsh1) harbors the same triple mutant ($PDGFRA^{D842V/V658A/G652E}$) that was found in the tumor biopsy. Both the cell line and the tumor biopsy had identical short tandem repeat profiles (Supplementary Fig. S4). This cell line was confirmed to express activated PDGFRA, which demonstrated biochemical resistance to avapritinib and other currently approved GIST therapies, as predicted by Ba/F3 modeling and clinical data (Fig. 3B). Further, Trsh1 cells showed activated PDGFRA-dependent signaling, which was inhibited by tanespimycin (Fig. 3C). These cells remained dependent on PDGFRA

A

B

C
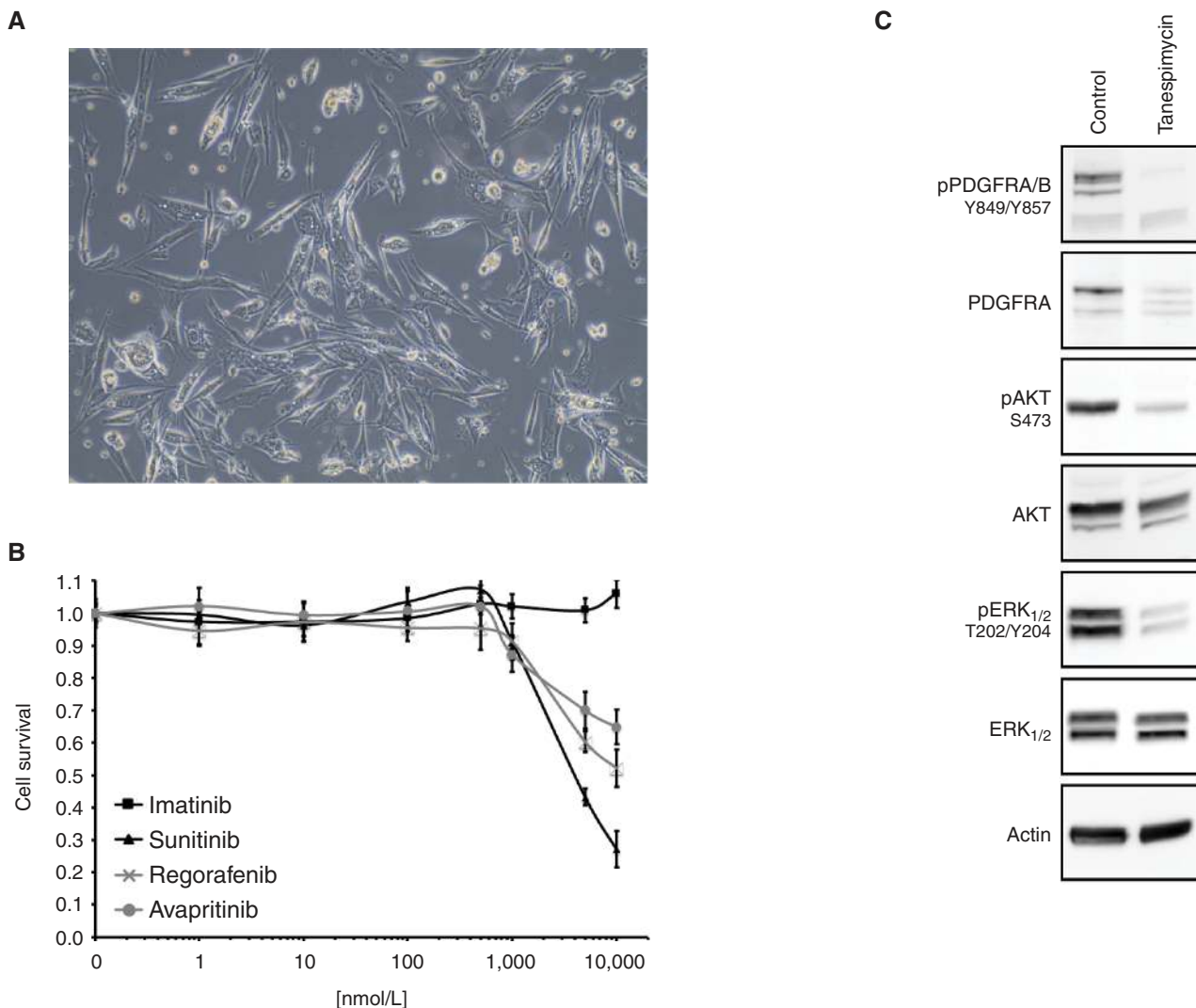
Figure 3. Patient-derived PDGFRA-mutant cell line demonstrates avapritinib resistance *in vitro*. Validation of Trsh1 cell line derived from a tumor from patient 1 with PDGFRA[D842V/V658A/G652E] mutation. **A,** Microscopic bright field image of Trsh1 growing at passage 19. **B,** Sulforhodamine B (SRB) assays to determine sensitivity of Trsh1 to approved KIT/PDGFRA inhibitors (some data points from this panel also appear in Fig. 5A). **C,** Immunoblot of Trsh1 cells untreated or treated (24 hours) with 500 nmol/L tanespimycin.

signaling, as knockdown of PDGFRA reduced cell viability (Supplementary Fig. S5A and S5B).

In Silico Modeling of Mutations in *PDGFRA*

Because the resistance mutations identified in these *PDGFRA*-mutant patients treated with avapritinib are novel, we evaluated potential structural explanations for the observed resistance. The kinase domain of type III receptor tyrosine kinases is subject to an equilibrium between inactive and active conformations (6). In the inactive state, the active site is blocked by the autoinhibitory conformation of the JM. To this end, D842 stabilizes the autoinhibited conformation within the AL (Fig. 4A). In the active and catalytically competent state, the JM is stabilized distant from the binding site by tyrosine side-chain phosphorylation, the helix αC takes an inward rotated position, and the AL adopts an extended

conformation with a characteristic DFG-*in* motif. This conformation is favored by the PDGFRA[D842V] mutation, which destabilizes the helical segments within the AL. Notably, in this conformation, type I inhibitors, such as avapritinib or crenolanib, can access the binding site for efficient kinase inhibition (6).

To better understand the conformational consequences of these mutations on protein structure, we performed *in silico* modeling for the most common PDGFRA mutants. Because the D842V mutation facilitates avapritinib binding, we assessed its binding mode using docking studies with a D842V-mutated molecular dynamics (MD) simulated homology model obtained for PDGFRA using KIT as the template structure. The binding mode is characterized by a hydrogen bond of the core scaffold with C677 within the hinge region. The fluorobenzyl moiety is wrapped
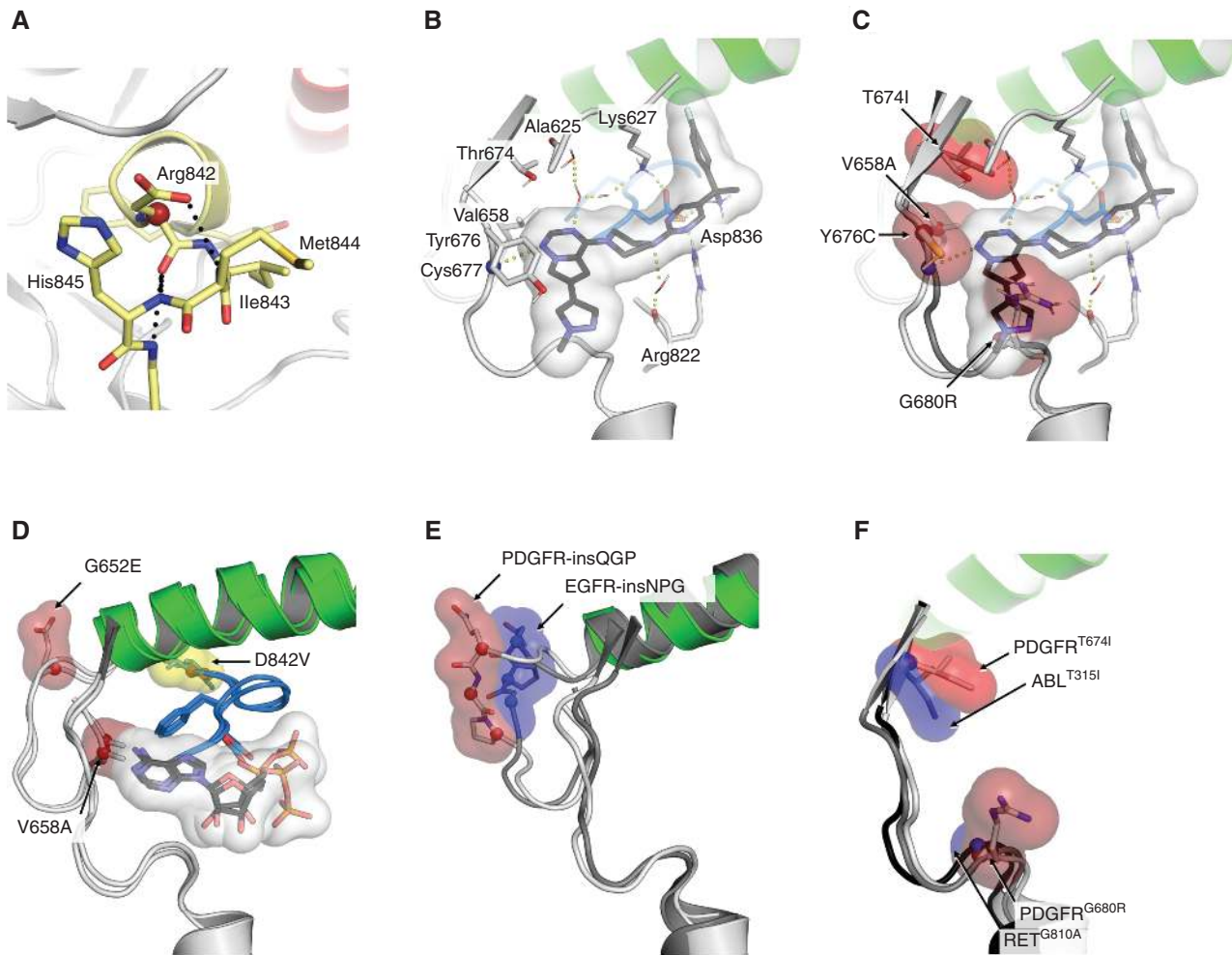
Figure 4. Conformational consequences of avapritinib-resistance *PDGFRA* mutations. *In silico* modeling of human PDGFRA. **A,** D842 within the AL (yellow) stabilizes the AL in the inactive DFG-out conformation by forming a network of polar contacts within the helical turn motif. **B,** Binding mode of avapritinib (MD simulation of a homology model, docked with avapritinib). **C,** Mutation G680R within the binding site sterically interferes with avapritinib binding. The mutations T674I (gray; PDB ID: 6A32) and V658A alter the hydrophobic properties of the binding cleft and result in reduced binding affinity. **D,** Alignment of MD simulation snapshots with ADP-bound PDGFRA harboring D842V/V658A or D842V/V658A/G652E mutations. **E,** Alignment of an MD simulation snapshot with PDGFRA-P653_H654insQGP mutation (gray and red) with similarly mutated EGFR-D770_N771insNPG (blue and gray; PDB ID: 4LRM). **F,** Alignment of PDGFR[T674I/G680R] (PDB ID: 6A32; G680R was applied using the Mutagenesis Wizard of PyMol) with ABL[T315I] (PDB ID: 3IK3) and RET[G810A] (PDB ID: 6NE7).

around the catalytic lysine (K627) and the DFG's aspartate (D836), which are engaged in polar contacts (Fig. 4B). This binding mode is incompatible with the mutation G680R within the kinase front pocket, which sterically interferes with avapritinib binding (Fig. 4C). The threonine-to-isoleucine mutation, T674I, was used to assess the gatekeeper moiety by an alignment with a crystal structure of PDGFRA[T674I] (PDB ID: 6A32, shown in gray; Fig. 4C), which disrupts a polar water-mediated network between A625, L627, and avapritinib. The valine at position 658 is in close interaction proximity to the avapritinib core binding site, and its substitution to alanine (V658A) might account for a loss in binding affinity resulting in drug resistance (Fig. 4C). Tyrosine at codon 676 serves as a "roof" for avapritinib binding and the interaction is lost with the cysteine substitution (Y676C; Fig. 4C).

Modeling of mutations located next to the regulatory helix αC, that is, PDGFRA[G652E] and PDGFRA[QGPins], however, did not result in an altered binding site (Fig. 4D and E). These mutations might act through altered dynamics of the adjacent helix or the binding motif recognized by interacting proteins. PDGFRA[QGPins], PDGFRA[T674I], and PDGFRA[G680R] correspond to analogous resistance mutations in other oncogenic kinases (Fig. 4E and F), further supporting the hypothesis that these mutations confer drug resistance.

Overcoming Resistance to Avapritinib

We evaluated whether mutations that emerged following treatment with avapritinib described herein are cross-resistant to other drugs or drug classes that are currently in clinical development for treatment of GIST. Crenolanib is another type I kinase inhibitor that has shown efficacy
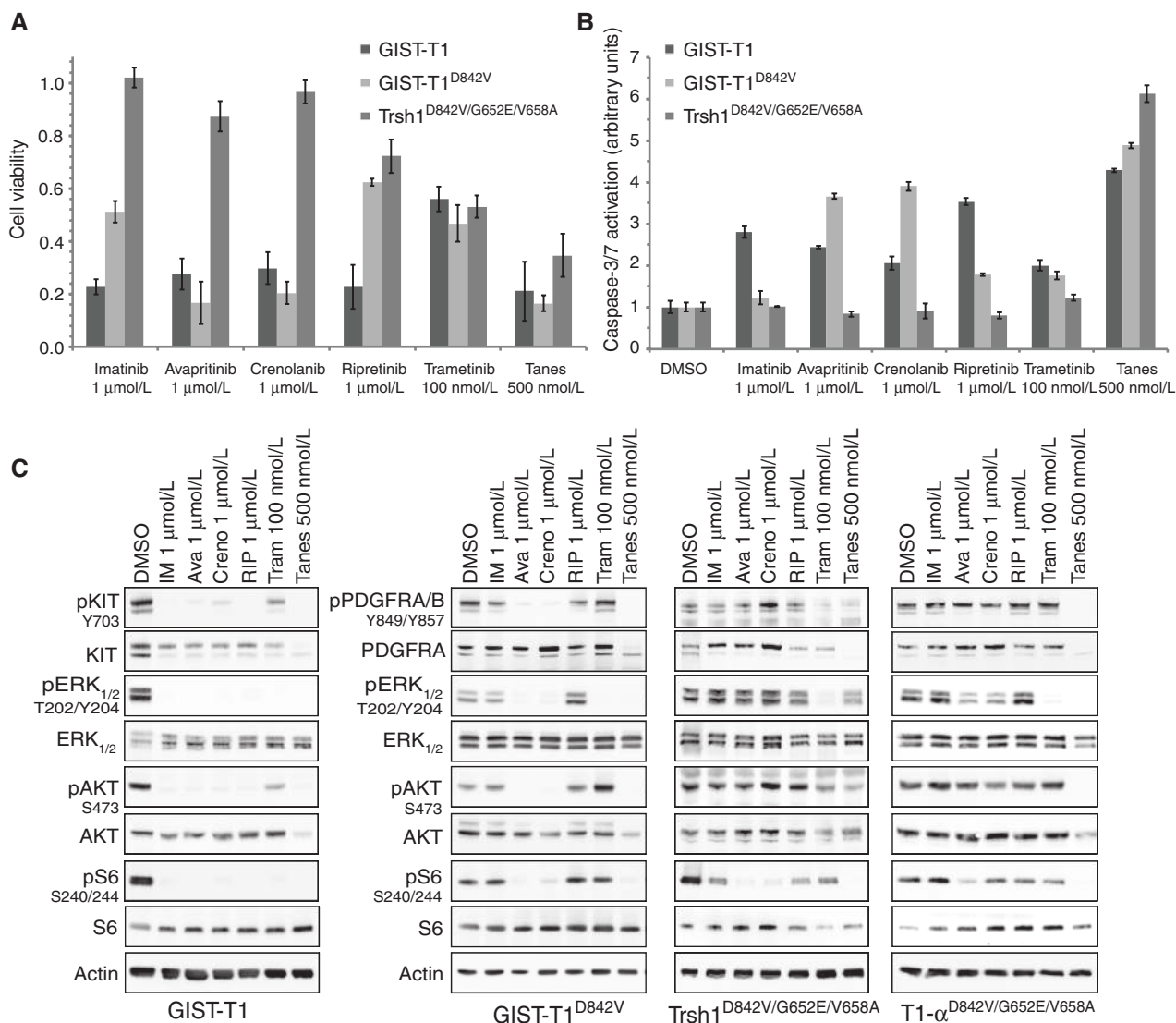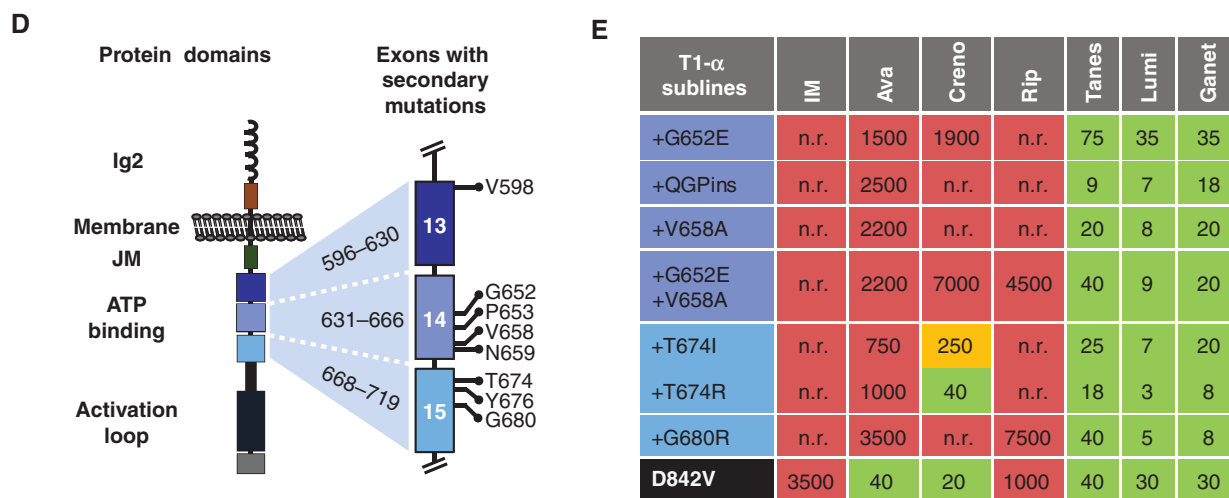
Figure 5. Focused drug screen in avapritinib-resistant GIST cell lines. **A,** SRB assays to compare the efficacy of different inhibitors in parental GIST-T1, GIST-T1^{D842V}, and Trsh1 (some data points from this panel also appear in Fig. 3A). **B,** Caspase Glo assays to determine induction of caspase cleavage for parental GIST-T1, GIST-T1^{D842V}, and Trsh1 to approved KIT/PDGFRA inhibitors or inhibitors in clinical development. **C,** Validation of substrate inhibition by western blot in parental GIST-T1, GIST-T1^{D842V}, Trsh1, and CRISPR-generated cell line T1-α$^{D842V/G652E/V658A}$. (*continued on next page*)

against PDGFRA^{D842V}, whereas ripretinib (DCC-2618) is a type II switch pocket inhibitor that recently was approved as a fourth-line treatment for advanced GIST (6, 21–23). Using our Ba/F3 models, we determined the effect of these additional kinase inhibitors on the various avapritinib resistance mutations to identify salvage therapies. In general, no other inhibitor outcompeted avapritinib against the secondary mutations examined (Supplementary Fig. S6A–S6M). One exception was the PDGFRA$^{D842V/V598F}$ mutation, which was resistant to all approved drugs but sensitive to crenolanib (IC$_{50}$ = 7 nmol/L; Supplementary Fig. S6B). Another exception was PDGFRA$^{I843-D846del/G680R}$, which was more sensitive to imatinib (IC$_{50}$ = 46 nmol/L) and ripretinib (IC$_{50}$ = 200 nmol/L), compared with an IC$_{50}$ value more than 3,000 nmol/L for avapritinib (Supplementary Fig. S6I).

To confirm these results in a GIST cellular context, we evaluated the effect of these drugs on the viability of our *PDGFRA*-mutant GIST cell line, Trsh1, and the reference cell line GIST-T1^{D842V}, expressing exogenous PDGFRA^{D842V}. GIST-T1^{D842V} was resistant to imatinib and ripretinib, but strongly inhibited by avapritinib and crenolanib (Fig. 5A). Unfortunately, Trsh1 (PDGFRA$^{D842V/G652E/V658A}$) exhibited resistance to all direct KIT/PDGFRA inhibitors, indicating these drugs cannot be used as salvage therapy for this specific mutation (Fig. 5A–C).

To assess further secondary mutations in a GIST context, we used CRISPR/Cas9-mediated gene editing to generate additional isogenic GIST-T1 sublines (designated T1-α), harboring mutations identified in patients within the endogenous *PDGFRA* gene (Fig. 5D and E). Parallel Cas9-mediated

D

Protein domains | Exons with secondary mutations

Ig2
Membrane
JM
ATP binding
Activation loop

596–630
631–666
668–719

13 — V598
14 — G652 / P653 / V658 / N659
15 — T674 / Y676 / G680

E

T1-α sublines	IM	Ava	Creno	Rip	Tanes	Lumi	Ganet
+G652E	n.r.	1500	1900	n.r.	75	35	35
+QGPins	n.r.	2500	n.r.	n.r.	9	7	18
+V658A	n.r.	2200	n.r.	n.r.	20	8	20
+G652E +V658A	n.r.	2200	7000	4500	40	9	20
+T674I	n.r.	750	250	n.r.	25	7	20
+T674R	n.r.	1000	40	n.r.	18	3	8
+G680R	n.r.	3500	n.r.	7500	40	5	8
D842V	3500	40	20	1000	40	30	30

Figure 5. *(Continued)* **D,** Overview of PDGFRA protein domains and exons involved in avapritinib resistance. Exons 13–15 (and their respective amino acid ranges), comprising the ATP-binding domain, are shown in more detail. Mutated amino acid residues discovered in patients and their approximate position are displayed. **E,** Secondary mutations discovered in patients were modeled in an isogenic cell line panel of GIST-T1. All cell lines carry the activating D842V mutation in exon 18. Additional resistance mutations were introduced into the ATP-binding domain. The pseudo heat map displays IC_{50} values (nmol/L) for different PDGFRA and HSP90 inhibitors in each subline: green = sensitive; yellow = intermediate; red = resistant. IM, imatinib; Ava, avapritinib; Creno, crenolanib; Rip, ripretinib; Tram, trametinib; Tanes, tanespimycin; Lumi, luminespib; Ganet, ganetespib; n.r. = not reached at 10,000 nmol/L.

knockout of mutant KIT led to a kinase switch and complete dependence upon mutant PDGFRA activity. Interrogating this panel for inhibitor sensitivity, we confirmed that although D842V-only mutants were sensitive to avapritinib and crenolanib, all clinically observed secondary mutations conferred resistance to avapritinib.

Based on these data, there is currently no direct inhibitor of PDGFRA available that potently inhibits these PDGFRA double and triple mutants. Possible exceptions could be mutations involving codons V598 and T674, where crenolanib may be active. Of note, the substitution at T674 was found in the context of an N659K primary mutation and not a D842V. Given the homology to KIT and ABL, we have additionally modeled both isoleucine and arginine substitutions as those are likely to be affected in the common D842V primary mutation (Fig. 5E; ref. 24).

In preclinical models of *KIT*-mutant GIST, inhibitors of HSP90 as well as inhibitors of KIT-activated signaling pathways can overcome resistance regardless of the secondary resistance mutation, but this has not been tested in *PDGFRA*-mutant GIST (20, 21). Notably, the HSP90 inhibitor tanespimycin (17-AAG), a derivative of the antibiotic geldanamycin, exerted potent activity in the multiresistant Trsh1 cell line (IC_{50} value: 70 nmol/L; Fig. 5A). Several other HSP90 inhibitors currently in clinical development show equal or more potent inhibition of triple-mutant PDGFRA, with luminespib (8 nmol/L) and ganetespib (60 nmol/L) exhibiting the lowest total growth inhibition (TGI; Supplementary Fig. S7). Furthermore, HSP90 inhibition was the only treatment associated with induction of apoptosis as measured by caspase-3/7 activation (Fig. 5B). Immunoblotting studies revealed potent inhibition of PDGFRA expression and signaling in the GIST-T1 parental and isogenic sublines, as well as Trsh1, upon tanespimycin treatment (Fig. 5C).

Notably, all cell lines in this panel also proved to be highly sensitive to HSP90 inhibition by tanespimycin (IC_{50} = 9–75 nmol/L), luminespib (IC_{50} = 5–35 nmol/L), and ganetespib (IC_{50} = 8–35 nmol/L; Fig. 5E). We further tested inhibitors of downstream pathways of PDGFRA as potential salvage treatments in avapritinib-resistant cells. In addition, trametinib, an inhibitor of MEK, inhibited growth of Trsh1 cells when near-complete target inhibition (pERK) was reached (100 nmol/L; Fig. 5A and C).

DISCUSSION

Activating mutations of the PDGFRA receptor tyrosine kinase were described more than 15 years ago, but until recently, no inhibitors with significant clinical activity against the notoriously resistant D842V mutation had been identified (4). Avapritinib has been shown to be a highly potent inhibitor of $PDGFRA^{D842V}$ with IC_{50} values in the subnanomolar range (15). A phase I trial of avapritinib revealed an 84% objective response rate and tumor shrinkage in more than 95% in this D842V-mutant cohort. Tumor shrinkage was evident even in the earliest dose cohorts of the escalation phase (16). In January 2020, avapritinib was approved by the FDA for the treatment of GIST with mutations in PDGFRA exon 18. Thus, avapritinib represents a therapeutic breakthrough with activity similar to that of imatinib against untreated, advanced *KIT* exon 11–mutant GIST. To date, only a minority of patients with *PDGFRA*-mutant tumors treated with avapritinib have developed resistance—underscoring the unique potency of avapritinib against the $PDGFRA^{D842V}$ activating mutation. However, patients whose tumors develop avapritinib resistance have extremely poor outcomes, with a median overall survival of 5.2 months after clinical progression and a median survival of <1 month after stopping avapritinib (Supplementary Fig. S1A). Understanding

mechanisms of avapritinib resistance and identification of salvage therapies are therefore of utmost importance in this subgroup of patients.

Currently, plasma sequencing of ctDNA has not been clinically validated for routine use in the management of patients with GIST but represents a potential tool for the early detection of resistant tumor clones. We report that the primary *PDGFRA* mutation (e.g., D842V) is detectable in the majority of patients using BEAMing or NGS technology, with the latter showing a slightly lower detection rate (Fig. 1A). To date, only a minority of patients have progressed on avapritinib, and because the protocol did not include mandatory post-progression plasma sample collection, only limited numbers of such samples were available. Nonetheless, we were able to identify resistance mutations via plasma sequencing in all seven patients for whom plasma was available. No secondary *PDGFRA* mutations were found in the pretreatment plasma sequencing samples of patients in the NAVIGATOR study. This supports the hypothesis that those mutations arise or are selected for during avapritinib treatment. It should be noted that the panel sequencing of baseline samples only included exons 12, 14, and 18 but not exon 13 or exon 15 of *PDGFRA*, as mutations in the latter exon had at the time not been reported. Post-progression tumor samples revealed only single resistance mutations whereas several mutations were found in the plasma samples (patients 1 and 2)—underscoring the polyclonal fashion of avapritinib resistance, which is well known for *KIT*-mutant GIST (25).

We are aware that clonal hematopoiesis may account for a wealth of mutations (up to 50%) that are found in the plasma. This is particularly important for ctDNA mutations found at low allelic frequencies. We have therefore reviewed analyses from plasma from 219 patients with GIST from the NAVIGATOR trial (Supplementary Table S2) with longitudinal sampling performed on a subset of patients. Twenty-seven patients were found to have *PDGFRA* mutations. Of those, 21 represented the known primary mutation and 6 patients had variants of unknown significance, none of which represented mutations that we have described above. At post-baseline assessments, the only mutations that were found were those reported herein. The plasma assay was also used to evaluate 817 plasma samples from 398 patients from the ARROW trial. No patient had a *PDGFRA* mutation, although the detection threshold was as low as 0.05% allelic frequency. In contrast, mutations that are characteristic of clonal hematopoiesis of indeterminate potential (e.g., DNMT3A mutations, JAK2[V617F]) were commonly observed with MAF as low as 0.08%.

In addition, baseline plasma samples from the phase III VOYAGER study for patients with imatinib- and sunitinib-resistant GIST (*n* = 430) were analyzed. The vast majority of patients in this trial had been treated with potent inhibitors of wild-type PDGFRA (imatinib and sunitinib at a minimum). Again, only two patients were found to have mutations in *PDGFRA* exon 18 in the plasma, both of whom had known *PDGFRA*-mutant GIST (i.e., patients 6 and 7; Table 1). We therefore conclude that the resistance mutations we found in the plasma are most likely due to avapritinib-resistant tumor clones.

We are the first to describe GIST with secondary mutations within *PDGFRA* (apart from D842V as a secondary mutation to an exon 12 *PDGFRA* mutation; ref. 23) and test their sensitivity to avapritinib and other kinase inhibitors using novel and unique *PDGFRA*-mutant models. In one avapritinib-resistant patient, we also report mutations that constitutively activate pathways typically activated by PDGFRA (PI3K and MAPK pathways), which have recently been described as genomic events that drive resistance in some cases of *KIT*-mutant GIST as well (18, 19). Our investigation focused on resistance conferred by secondary *PDGFRA* mutations using our novel *PDGFRA*-mutant models. Although secondary mutations within the ATP-binding pocket and the AL are well understood in *KIT*-mutant GIST (11, 26–28), resistance mutations have not been well described in *PDGFRA*-mutant GIST, even in patients with imatinib-sensitive *PDGFRA* mutations (29). Here, we report that *PDGFRA*-mutant GIST tumors with clinical avapritinib resistance utilize similar escape mechanisms as those found in imatinib-resistant KIT-mutant GIST.

The secondary mutations that confer avapritinib resistance described in this study were found exclusively in exons 13, 14, and 15, which encode the ATP-binding pocket. These *PDGFRA* resistance mutations are novel both in the context of PDGFRA-inhibitory treatment but also in a pan-cancer context. A query of The Cancer Genome Atlas database (10,967 samples from 10,953 patients across 32 tumor histologies) revealed no mutations at *PDGFRA* codons 598, 652, 658, 674, or 676. A single mutation at codon 680 (G680E) was seen in a patient with uterine serous carcinoma. A second query in a nonredundant data set of 47,005 samples from 178 trials yielded a single *PDGFRA* mutation Y676H in a patient with uterine endometrioid cancer. All other reported *PDGFRA* mutations were mutations in codon 842 (V/Y/I) that were found in GIST (*n* = 9), glioblastomas (*n* = 2), high-grade gliomas (*n* = 1), and neuroblastomas (*n* = 1).

In silico studies modeling secondary mutations found in patient-derived samples demonstrated steric hindrance with avapritinib. Notably, some *PDGFRA* secondary mutations occur at homologous residues to those of typical resistance mutations in other oncogenic kinases. The PDGFRA[V658A] mutant corresponds to KIT[V654A] and PDGFRA[T674I] to the KIT gatekeeper mutant T670I, which again corresponds with BCR–ABL T315I found in chronic myelogenous leukemia (CML; refs. 12, 30). The G680R secondary mutation is predicted to increase resistance to avapritinib due to a steric clash resulting in a solvent-front mutation (Fig. 4C). Notably, PDGFRA[G680R] resembles the substitution mutation found in drug-resistant RET-driven cancers (G810A; Fig. 4F; ref. 31). Solvent-front mutations involving a glycine have also been described for EGFR (G796S), ALK (G1202R), TRKA (G595R), TRKC (G623R), and ROS (G2032R; refs. 32–36). Interestingly, this mutation conferred the strongest resistance to imatinib in our biochemical assays, but its resistance to imatinib was dependent upon the context of the primary mutation, such that imatinib outperformed avapritinib in the context of PDGFRA[I843-D846del/G680R] (Supplementary Fig. S6I). In contrast with the resistance mutations described above, V598F does not directly interfere with the inhibitor, and the side chain is far from the drug-binding site. However, V598 is located adjacent to the glycine-rich loop, which is a highly flexible element and crucial for substrate and ligand

American Association for Cancer Research

binding (37, 38). We therefore assume an influence of V598F on the dynamics of the G-rich loop results in drug resistance.

Patient 7, harboring a non-D842V primary mutation, responded to avapritinib despite a pretreatment G680R secondary mutation found at low allelic frequency in plasma only. As we did not find evidence for these mutations to reflect clonal hematopoiesis, it is likely that this clone represented a small fraction of the patient's tumor load and would not prevent the overall disease assessment from achieving a partial remission, before continued expansion of the clone resulted in clinical progression. The median allelic frequency of the primary mutation was >10 times higher than the resistance mutation. This case underscores that although plasma sequencing is a powerful technology for discovery of resistance mutations, it is not yet a validated predictive marker.

Although most of the secondary resistance mutations were point mutations, $PDGFRA^{D842V/QGPins}$ also conferred moderate resistance to avapritinib (Figs. 2 and 5). Importantly, it closely aligns with an insertion mutation (D770_N771insNPG) found in a subset of patients with *EGFR*-mutant lung cancer (Fig. 4E). This insertion has been described to be at the pivot point of the helix αC, and the inserted residues sterically inhibit the reorientation of the helix αC characteristic of the inactive state (39) and interfere with an adjacent electrostatic switch interaction that is proposed to stabilize an inactive EGFR dimer (40). Our data also show that resistance mutations emerging from imatinib treatment in patients with imatinib-sensitive *PDGFRA* mutations may cause cross-resistance to avapritinib (patient 5). Studying imatinib resistance in patients with non–D842V-mutant tumors will therefore be important to better understand cross-resistance against PDGFRA inhibitors. Patient 1 was found to have a compound mutation in exon 14. This is noteworthy, as compound mutations have been described for BCR–ABL in CML (41), rarely in the context of KIT (11) and not yet in PDGFRA-driven GIST. Exome sequencing of the resistant tumor revealed this mutation to be homozygous (Supplementary Table S1), confirming that most, if not all, mutations must be in *cis*. This was also true for the Trsh1 cell line. Notably, looking at individual NGS reads reveals that V652E and V658A are observed both in *cis* and in *trans* in the aligned reads that span both codons ("spanning reads"). This is consistent with multiple mutational events (i.e., independent development of V652E and V658A as well as sequential mutations in the same allele). Fitting to the observation of multiple events, one post-progression plasma sample of this same patient showed two different base exchanges, leading to the same G680R substitution mutation albeit at highly different allelic frequencies (Table 1). Our functional studies show that the compound mutation is more resistant than the V658A mutation alone, which would support the hypothesis that the mutations occurred sequentially.

Apart from avapritinib, two other drugs show evidence of activity against *PDGFRA*-mutant GIST. Crenolanib, a benzimidazole compound, has been reported to be a potent inhibitor of PDGFRA and PDGFRB and was the first drug to show promising activity against D842V mutants *in vitro*, and preliminary clinical data also reported activity in patients (23, 42). A randomized phase III trial is currently ongoing (NCT02847429). Ripretinib (DCC-2618), a "switch-control" inhibitor of KIT and PDGFRA, has been shown to potently inhibit PDGFRA fusions and intragenic point mutants in biochemical assays (21). We found cross-resistance for ripretinib and crenolanib in most avapritinib-resistant models—in fact, ripretinib showed low potency against all D842V mutations, even the primary mutation, when tested in a GIST-specific context (Fig. 5E; $IC_{50} \geq 1,000$ nmol/L). To our knowledge, clinical outcomes for ripretinib treatment of D842V-mutant patients have not yet been reported. Of note, T1-α-$^{D842V/T674I}$ had biochemical resistance to avapritinib and crenolanib. For the sublines with secondary mutations in codon 674, crenolanib showed an IC_{50} of 250 nmol/L for the isoleucine (T674I) and 40 nmol/L for the arginine substitution (T674R). This suggests that crenolanib might have clinical activity against lesions harboring this particular resistance mutation. The IC_{50} for avapritinib was at 750 nmol/L, which is considered above clinically relevant levels. In agreement with these observations, patient 5, who had a secondary T674R mutation, did not respond to avapritinib at a dose of 200 mg daily.

Of note, we did not find evidence for escape mechanisms apart from resistance mutations in PDGFRA and its downstream signaling pathways. In patient 1, whole-exome sequencing studies comparing baseline and post-progression tumor samples revealed no other acquired mutations than those found in *PDGFRA*. After filtering for nonsynonymous variants and likely nonpathogenic variants, only *PDGFRA* secondary resistance mutations remained as differentially mutated genes.

Our results strongly support the hypothesis that for avapritinib-resistant GIST, salvage treatments should focus on improving PDGFRA inhibitors or combining avapritinib with inhibitors of downstream effectors. Notably, patient-derived cells harboring PDGFRA triple mutations remain strongly dependent on the oncogenic signal of PDGFRA (Supplementary Fig. S5). PDGFRA, just like KIT, is a client of the HSP90 chaperone (43). Consequently, HSP90 inhibition completely abrogated PDGFRA phosphorylation—regardless of the secondary or tertiary resistance mutations (Fig. 5C). Both *KIT*-mutant and *PDGFRA*-mutant GIST seem uniquely dependent on their respective kinases, and, with both being substrates for HSP90, an indirect inhibition could represent a rational strategy. Although first- and second-generation HSP90 inhibitors have failed to provide lasting clinical benefit in GIST, metabolic studies have provided proof-of-concept that efficient KIT inhibition can be achieved at least in the short term. Very recently, a novel HSP90 inhibitor has been found active in *KIT*-mutant GIST (44). Therefore, next-generation HSP90 inhibitors remain a valid therapeutic concept warranting further preclinical and clinical testing for *PDGFRA*-mutant GIST as well.

Notably, in GIST cells harboring *KIT* mutations, *PDGFRA* regulates proliferation by stabilizing ETV1 (45), and this stabilization of ETV1 expression is dependent on ERK pathway signaling (46, 47). We found that inhibition of MEK/ERK using trametinib resulted in effective growth inhibition *in vitro* even in highly avapritinib-resistant sublines. Although clinical trials using MEK inhibitors have yet shown modest activity in *KIT*-mutant GIST (48), these results further underscore that avapritinib-resistant tumors remain dependent on oncogenic PDGFRA signaling.

In conclusion, our data show for the first time that resistance mechanisms in avapritinib-resistant *PDGFRA*-mutant GIST mirror those seen in imatinib-resistant KIT-mutant GIST. These consist of secondary *PDGFRA* mutations, particularly in the kinase domain, and less commonly mutations that constitutively activate PDGFRA downstream signaling intermediates. Future diagnostic sequencing panels should include *PDGFRA* exons 13, 14, and 15 for the detection of resistance mutations. Based on our *in vitro* studies, most but not all of these mutations appear to confer cross-resistance to other PDGFRA inhibitors currently in clinical development. Our data also provide first evidence that the oncogenic PDGFRA signal remains the dominant oncogenic driver at the time of progression and that salvage treatments should focus on improving PDGFRA-inhibitory strategies and also targeting the PDGFRA-dependent RAS–RAF–MAPK pathway.

METHODS

Patients

The NAVIGATOR trial is a phase I dose-escalation trial investigating avapritinib in patients with metastatic GIST refractory to IM and at least one other kinase inhibitor or a D842V mutation in PDGFRA. Eligibility criteria included provision of written informed consent, age ≥18 years, Eastern Cooperative Oncology Group performance status ≤2 and adequate end-organ function. Patient 1, a 67-year-old man, patient 2, a 76-year-old man, and patient 3, a 64-year-old man, all had a primary *PDGFRA*[D842V] mutation and did not receive any previous systemic treatment. Patient 4 is a 70-year-old man with a primary DIMH-PDGFRA mutation in exon 18 who was included in the trial after having failed imatinib, sunitinib, and regorafenib treatment. Patient 5 is a 52-year-old man with a primary *PDGFRA*[N659K] mutation in *PDGFRA* exon 14, who gained a secondary T674R mutation following imatinib and sunitinib treatment. Radiologic response to avapritinib was measured according to mRECIST criteria version 1.1 (49), and RECIST terms were used to describe tumor lesion measurements. Patient 6, who had a primary, imatinib-sensitive D842_D846delinsE mutation, had discontinued imatinib for unknown reasons and progressed on sunitinib when the plasma sample was taken. Patient 7 had a D842_D846delinsV *PDGFRA* primary mutation and had already progressed on imatinib, sunitinib, and sorafenib before plasma sequencing. Two secondary mutations reported within the deleted segment (M844I and M844K) were interpreted as sequencing artifacts.

Sequencing Analyses

During the escalation phase of the NAVIGATOR trial, mutant plasma DNA from patients with PDGFRA mutations was analyzed by BEAMing analyses and during the expansion phase using the PlasmaSelect gene panel assay (Personal Genome Diagnostics PGDx). BEAMing is a digital PCR approach that measures 5 specific PDGFRA mutations (V561D, T674I, D842V, D842-H845del, and I843_D846del). Sequenced DNA was aligned to the RAS sequence within the reference human genome to report mutations with a sensitivity of 0.1% mutant DNA, which is the limit of detection for the assay (50). The PlasmaSelect is an NGS-based panel sequencing assay that covers full coding sequences of both PDGFRA and KIT as well as 58 additional genes that may confer resistance to tyrosine kinase inhibitors. Plasma sequencing was performed on cycle 1 day 1 as well as at the end of treatment, when possible.

For 3 patients, post-progression samples were also analyzed using the Guardant360 system, which covers 73 genes, including *KIT*, *PDGFRA*, and common genes associated with tyrosine kinase inhibitor resistance as described previously (51).

For the VOYAGER trial (NCT03465722), plasma sequencing was performed at screening using Guardant360. For the ARROW trial (NCT03037385), plasma was analyzed using the PGDx PlasmaSelect64 assay, which evaluates a targeted panel of 64 cancer genes including *PDGFRA*.

Novel sequence variants were deposited at the Sequence Read Archive (SRA accession numbers SAMN16095462, SAMN16095463, SAMN16095464, SAMN16095465, SAMN16226685, SAMN16226686, and PRJNA664602).

Whole-Exome Sequencing

Whole-exome sequencing was done in a Clinical Laboratory Improvement Amendments (CLIA)–compliant laboratory (Genewiz). Results were filtered for somatic, nonsynonymous mutations and for variants that were found in the OMIM or OMIA databases. Variants were removed if the MAF was greater than 5% in the population or was reported in the 1000 genomes project (52).

Cell Lines, Reagents, and Antibodies

GIST-T1 and Trsh1 were established from human metastatic GIST. GIST-T1 contains a 57-bp deletion in KIT exon 11 (47). Trsh1 was established from tumor tissue that was obtained by a diagnostic biopsy of a growing lesion following avapritinib treatment (patient 1). The cell line harbors a primary *PDGFRA* exon 18 D842V mutation and two intra-allelic secondary mutations in exon 14 (V658A and G652E). GIST-T1[D842V] is a subline of GIST-T1 that was created by transducing cells with D842V-mutant *PDGFRA*. Endogenous *KIT* was knocked out using CRISPR/Cas9. Knockout was verified at protein and DNA levels. All cell lines were grown in Iscove's Modified Dulbecco's Medium with 10% FBS at 37°C and 5% CO$_2$. All cell lines were regularly authenticated by sequencing of endogenous mutations in *KIT*, confirmation of *KIT* expression, and response to KIT inhibitor treatment. In the course of this study, all cell lines were regularly tested for *Mycoplasma* contamination by PCR and the MycoAlert Mycoplasma Detection Kit (Lonza).

Generation of Ba/F3 Cell Lines

Ba/F3 cells were grown in RPMI-1640 medium with 10% FBS at 37°C and 5% CO$_2$. Lentiviruses were produced by transient transfection of HEK-293T cells with ViraPower Lentiviral Packaging Mix (Invitrogen, #K497500) plus the pLENTI-C-Myc-DDK-IRES-Neo vector (Origene) containing full-length *PDGFRA* cDNA encoding each of the described mutations. Ba/F3 cells were then transduced with filtered lentivirus and polybrene via spinoculation and supplemented with murine IL3 (Cell Signaling Technology, #8923C). Transduced, IL3-dependent Ba/F3 cells were then selected for 1 week in G418 (Sigma, #A1720). In order to generate IL3-independent clones, G418-resistant Ba/F3 cells were plated in limiting dilutions in the absence of IL3 and grown for 1 to 3 weeks (48). Full sequencing of the *PDGFRA* cDNA was performed for each clonal IL3-independent Ba/F3 cell line. The PDGFRA mutation P653_H654insQGP is abbreviated as QGPins in the text and figures.

Gene Editing by CRISPR/Cas9

Further cell lines with endogenous *PDGFRA* mutations (T1α[D842V], T1α[D842V/QGPins], T1α[D842V/G652E], T1α[D842V/V658A], T1α[D842V/G652E/V658A], T1α[D842V/T670I], T1α[D842V/G680R]) were generated by CRISPR/Cas9-mediated gene editing, as described previously (18), with the following deviations: We used recombinant Cas9 from IDT Labs (60 µmol/L) in a 1:2 ratio with specific single guide RNA (sgRNA). First, *PDGFRA*[D842V] was introduced into parental GIST-T1, and cells were selected with IM 200 nmol/L until outgrowth of a resistant population, which carried heterozygous *PDGFRA*[D842V]. In a second round of editing,

AACR American Association for Cancer Research

one sgRNA specific for *PDGFRA*-resistance mutations (exons 14 and 15) and an ssODN template to introduce the desired mutation (P653_H654insQGP, G652E, V658A, G652E/V658A, T674I, T674R, and G680R, respectively) was combined with a guide targeting exon 1 (for G652E, G652E/V658A, T674I, and G680R) or mutant exon 11 (for D842V-only, QGPins, and V658A) of KIT. Cells were then treated with avapritinib 100 nmol/L, and after outgrowth of a resistant population, single-cell clones were derived. Heterozygous D842V and in *cis* secondary mutations as well as frameshift mutations in mutant exon 1 and 11 of *KIT* were confirmed by Sanger sequencing and/or next-generation panel sequencing. Strong reduction of KIT expression and phosphorylation were confirmed by Western blotting. For a complete list of sequences used in CRISPR/Cas9 experiments, see Supporting Information.

CHO Transfection

Chinese Hamster Ovary (CHO) cells were cultured in FK12 medium + 10% FBS at 37°C and 5% CO_2. Cells were plated and transfected with various *PDGFRA*-mutant expressing plasmids (pcDNA 3.1+). After 24 hours, cells were treated with drug at indicated doses for 90 minutes and then harvested for immunoblotting.

SRB Cell Viability Assay

The sulforhodamine B (SRB) assay was used according to the method of Skehan and colleagues (53). Cells were plated at 5,000–10,000 cells/well in a 96-well flat-bottom plate and cultured for 24 hours. An untreated control plate was measured at the time of treatment for normalization, that is, to define the concentration of TGI and half TGI (TGI_{50}). Cells were then incubated with media containing inhibitors or solvent control (DMSO). After 72 hours, cells were fixed and stained with SRB (0.4%, Sigma-Aldrich), and absorption was measured with a Genion luminometer (Tecan). All measurements were carried out in triplicate/quadruplicate wells for at least two times, and a representative example is shown.

CellTiter-Glo Cell Viability Assay

Cells were plated, transfected, and incubated in opaque 96-well plates (Corning). Cell viability was measured using the CellTiter-Glo reagent (Promega) according to the manufacturer's instructions.

Assessment of Apoptosis

For assessment of caspase-3/7 activation by Caspase Glo luminescent assay (Promega), cells were prepared as above and treated for 16 hours. Then Caspase Glo reagent was added according to the manufacturer's protocol, and resulting luminescence was measured.

Western Blotting

Ba/F3 and CHO drug experiments were performed for 90 minutes before harvesting whole-cell protein lysates for immunoblotting. For GIST cells, whole-cell protein lysates were prepared as previously described (54). Protein concentrations were determined with the Bio-Rad Protein Assay (Bio-Rad Laboratories). Proteins were separated by SDS/PAGE as described by Laemmli and colleagues (55) and transferred to Hybond-P membranes (Amersham Pharmacia Biotech). Changes in protein expression and phosphorylation as visualized by chemiluminescence (ECL chemi-luminescent reagent, Amersham Pharmacia Biotech) were captured and quantified using a FUJI LAS3000 system with Science Lab 2001 ImageGauge 4.0 software (Fujifilm Medial Systems).

PDGFRA Knockdown Studies

For an inducible knockdown of the *PDGFRA* gene, the Trsh1 cells were transduced with lentiviral particles: one control (nontargeting) and three *PDGFRA* ORF-targeting shRNAs in doxycycline-inducible SMARTvectors (GE Healthcare/Dharmacon, product #V3SH11255-01EG5156). The virus was packaged using the 293T cell line transfected with second-generation lentiviral packaging plasmids psPAX2 and pMD2. Selection for cells harboring expressable proviral integrants was started 3 days after transduction with puromycin at 2 µg/mL.

In Silico Modeling Studies for PDGFRA

The KIT crystal structure with the PDB ID 1PKG was used to generate homology models of PDGFRA mutants in the activated state (D842V, D842V/V658A, D842V/V658A/G652E, and D842V/P653_H654insQGP). The homology modeling was performed with the "Homology Modelling" tool as implemented in MOE2015 (Molecular Operating Environment) Version 2015.10; Chemical Computing Group ULC). We generated 10 backbone models and 25 side-chain models per protein and retained ADP and the Mg^{2+} ion of the template structure as environment for induced fit.

For the validation of the homology models, the generated PDGFRA structures were subjected to 400 ns MD simulations using the software package AMBER2018 (56). Details regarding the MD simulations can be found elsewhere (52). The ion parameters by Li and colleagues were used (57). The parameters for ADP (58) were obtained from the AMBER parameter database (http://research.bmh.manchester.ac.uk/bryce/amber/). The resulting MD snapshots were clustered according to the RMSD of the ATP binding site–constituting residues using the hierarchical agglomerative approach (average linkage, RMSD threshold = 1.5 Å) as implemented in CPPTRAJ (59), and representative snapshots were extracted.

The representative snapshots of the PDGFRA^{D842V} structure were used for a molecular ensemble docking of avapritinib with GOLD (60). We used all residues within 10 Å of ADP as the binding site definition and performed 100 GA runs, and the "early termination" option was disabled. Apart from that, the default settings were applied. The resulting binding modes were visually inspected and the binding mode exerting the most favorable interactions with the binding site and showing the lowest number of clashes was chosen for a subsequent MD simulation.

The MD simulation of the hypothetical avapritinib binding mode in PDGFRA^{D842V} was performed as described above using the AMBER2018 package. Avapritinib was parameterized using the GAFF force field (61) and AM1-BCC charges with antechamber (58). The simulation was performed until a stable binding mode of avapritinib was observed (1000 ns). PyMOL was used for generating the figures (The PyMOL Molecular Graphics System, Version 2.2.0; Schrödinger, LLC).

Reagents and Antibodies

A list of reagents/drugs and antibodies is provided in Supplementary Table S3.

Authors' Disclosures

Authors' Contributions

Acknowledgments

REFERENCES

1. Pogorzelski M, Falkenhorst J, Bauer S. Molecular subtypes of gastrointestinal stromal tumor requiring specific treatments. Curr Opin Oncol 2016;28:331–7.
2. Min KW, Leabu M. Interstitial cells of Cajal (ICC) and gastrointestinal stromal tumor (GIST): facts, speculations, and myths. J Cell Mol Med 2006;10:995–1013.
3. Hirota S, Isozaki K, Moriyama Y, Hashimoto K, Nishida T, Ishiguro S, et al. Gain-of-function mutations of c-kit in human gastrointestinal stromal tumors. Science 1998;279:577–80.
4. Heinrich MC, Corless CL, Duensing A, McGreevey L, Chen CJ, Joseph N, et al. PDGFRA activating mutations in gastrointestinal stromal tumors. Science 2003;299:708–10.
5. Corless CL, McGreevey L, Haley A, Town A, Heinrich MC. KIT mutations are common in incidental gastrointestinal stromal tumors one centimeter or less in size. Am J Pathol 2002;160:1567–72.
6. Klug LR, Kent JD, Heinrich MC. Structural and clinical consequences of activation loop mutations in class III receptor tyrosine kinases. Pharmacol Ther 2018;191:123–34.
7. Heinrich MC, Corless CL, Demetri GD, Blanke CD, Von Mehren M, Joensuu H, et al. Kinase mutations and imatinib response in patients with metastatic gastrointestinal stromal tumor. J Clin Oncol 2003;21:4342–9.
8. Li B, Garcia CS, Marino-Enriquez A, Grunewald S, Wang Y, Bahri N, et al. Conjoined hyperactivation of the RAS and PI3K pathways in advanced GIST. J Clin Oncol 2016;34:e22520.
9. Nannini M, Urbini M, Astolfi A, Biasco G, Pantaleo MA. The progressive fragmentation of the KIT/PDGFRA wild-type (WT) gastrointestinal stromal tumors (GIST). J Transl Med 2017;15:113.
10. Shi X, Sousa LP, Mandel-Bausch EM, Tome F, Reshetnyak AV, Hadari Y, et al. Distinct cellular properties of oncogenic KIT receptor tyrosine kinase mutants enable alternative courses of cancer cell inhibition. Proc Natl Acad Sci U S A 2016;113:E4784–93.
11. Heinrich MC, Corless CL, Blanke CD, Demetri GD, Joensuu H, Roberts PJ, et al. Molecular correlates of imatinib resistance in gastrointestinal stromal tumors. J Clin Oncol 2006;24:4764–74.
12. Debiec-Rychter M, Cools J, Dumez H, Sciot R, Stul M, Mentens N, et al. Mechanisms of resistance to imatinib mesylate in gastrointestinal stromal tumors and activity of the PKC412 inhibitor against imatinib-resistant mutants. Gastroenterology 2005;128:270–9.
13. Cassier PA, Fumagalli E, Rutkowski P, Schoffski P, Van Glabbeke M, Debiec-Rychter M, et al. Outcome of patients with platelet-derived growth factor receptor alpha-mutated gastrointestinal stromal tumors in the tyrosine kinase inhibitor era. Clin Cancer Res 2012;18:4458–64.
14. Indio V, Astolfi A, Tarantino G, Urbini M, Patterson J, Nannini M, et al. Integrated molecular characterization of gastrointestinal stromal tumors (GIST) harboring the rare D842V mutation in PDGFRA gene. Int J Mol Sci 2018;19:732.
15. Evans EK, Gardino AK, Kim JL, Hodous BL, Shutes A, Davis A, et al. A precision therapy against cancers driven by KIT/PDGFRA mutations. Sci Transl Med 2017;9:eaao1690.
16. Heinrich MC, Jones RL, von Mehren M, Schoffski P, Serrano C, Kang YK, et al. Avapritinib in advanced PDGFRA D842V-mutant gastrointestinal stromal tumour (NAVIGATOR): a multicentre, open-label, phase 1 trial. Lancet Oncol 2020;21:935–46.

American Association for Cancer Research

17. Namlos HM, Boye K, Mishkin SJ, Baroy T, Lorenz S, Bjerkehagen B, et al. Noninvasive detection of ctDNA reveals intratumor heterogeneity and is associated with tumor burden in gastrointestinal stromal tumor. Mol Cancer Ther 2018;17:2473–80.

18. Muhlenberg T, Ketzer J, Heinrich MC, Grunewald S, Marino-Enriquez A, Trautmann M, et al. KIT-dependent and KIT-independent genomic heterogeneity of resistance in gastrointestinal stromal tumors – TORC1/2 inhibition as salvage strategy. Mol Cancer Ther 2019;18:1985–96.

19. Serrano C, Wang Y, Marino-Enriquez A, Lee JC, Ravegnini G, Morgan JA, et al. KRAS and KIT gatekeeper mutations confer polyclonal primary imatinib resistance in GI stromal tumors: relevance of concomitant phosphatidylinositol 3-kinase/AKT dysregulation. J Clin Oncol 2015;33:e93–6.

20. Lierman E, Folens C, Stover EH, Mentens N, Van Miegroet H, Scheers W, et al. Sorafenib is a potent inhibitor of FIP1L1-PDGFRalpha and the imatinib-resistant FIP1L1-PDGFRalpha T674I mutant. Blood 2006;108:1374–6.

21. Smith BD, Kaufman MD, Lu WP, Gupta A, Leary CB, Wise SC, et al. Ripretinib (DCC-2618) is a switch control kinase inhibitor of a broad spectrum of oncogenic and drug-resistant KIT and PDGFRA variants. Cancer Cell 2019;35:738–51.

22. Blay JY, Serrano C, Heinrich MC, Zalcberg J, Bauer S, Gelderblom H, et al. Ripretinib in patients with advanced gastrointestinal stromal tumours (INVICTUS): a double-blind, randomised, placebo-controlled, phase 3 trial. Lancet Oncol 2020;21:923–34.

23. Heinrich MC, Griffith D, McKinley A, Patterson J, Presnell A, Ramachandran A, et al. Crenolanib inhibits the drug-resistant PDGFRA D842V mutation associated with imatinib-resistant gastrointestinal stromal tumors. Clin Cancer Res 2012;18:4375–84.

24. Carter TA, Wodicka LM, Shah NP, Velasco AM, Fabian MA, Treiber DK, et al. Inhibition of drug-resistant mutants of ABL, KIT, and EGF receptor kinases. Proc Natl Acad Sci U S A 2005;102:11011–6.

25. Wardelmann E, Thomas N, Merkelbach-Bruse S, Pauls K, Speidel N, Buttner R, et al. Acquired resistance to imatinib in gastrointestinal stromal tumours caused by multiple KIT mutations. Lancet Oncol 2005;6:249–51.

26. Desai J, Shankar S, Heinrich MC, Fletcher JA, Fletcher CD, Manola J, et al. Clonal evolution of resistance to imatinib in patients with metastatic gastrointestinal stromal tumors. Clin Cancer Res 2007;13:5398–405.

27. Heinrich MC, Corless CL, Liegl B, Fletcher CD, Raut CP, Donsky R, et al. Mechanisms of sunitinib malate (SU) resistance in gastrointestinal stromal tumors (GISTs). Proc Am Soc Clin Oncol 2007;25:10006.

28. Liegl B, Kepten I, Le C, Zhu M, Demetri GD, Heinrich MC, et al. Heterogeneity of kinase inhibitor resistance mechanisms in GIST. J Pathol 2008;216:64–74.

29. Corless CL, Schroeder A, Griffith D, Town A, McGreevey L, Harrell P, et al. PDGFRA mutations in gastrointestinal stromal tumors: frequency, spectrum and in vitro sensitivity to imatinib. J Clin Oncol 2005;23:5357–64.

30. Branford S, Rudzki Z, Walsh S, Grigg A, Arthur C, Taylor K, et al. High frequency of point mutations clustered within the adenosine triphosphate-binding region of BCR/ABL in patients with chronic myeloid leukemia or Ph-positive acute lymphoblastic leukemia who develop imatinib (STI571) resistance. Blood 2002;99:3472–5.

31. Liu X, Shen T, Mooers BHM, Hilberg F, Wu J. Drug resistance profiles of mutations in the RET kinase domain. Br J Pharmacol 2018;175:3504–15.

32. Drilon A, Nagasubramanian R, Blake JF, Ku N, Tuch BB, Ebata K, et al. A next-generation TRK kinase inhibitor overcomes acquired resistance to prior TRK kinase inhibition in patients with TRK fusion-positive solid tumors. Cancer Discov 2017;7:963–72.

33. Ignatius Ou SH, Azada M, Hsiang DJ, Herman JM, Kain TS, Siwak-Tapp C, et al. Next-generation sequencing reveals a Novel NSCLC ALK F1174V mutation and confirms ALK G1202R mutation confers high-level resistance to alectinib (CH5424802/RO5424802) in ALK-rearranged NSCLC patients who progressed on crizotinib. J Thorac Oncol 2014;9:549–53.

34. Klempner SJ, Mehta P, Schrock AB, Ali SM, Ou SI. Cis-oriented solvent-front EGFR G796S mutation in tissue and ctDNA in a patient progressing on osimertinib: a case report and review of the literature. Lung Cancer 2017;8:241–7.

35. Drilon A, Ou SI, Cho BC, Kim DW, Lee J, Lin JJ, et al. Repotrectinib (TPX-0005) is a next-generation ROS1/TRK/ALK inhibitor that potently inhibits ROS1/TRK/ALK solvent-front mutations. Cancer Discov 2018;8:1227–36.

36. Yun MR, Kim DH, Kim SY, Joo HS, Lee YW, Choi HM, et al. Repotrectinib exhibits potent antitumor activity in treatment-naive and solvent-front-mutant ROS1-rearranged non-small cell lung cancer. Clin Cancer Res 2020;26:3287–95.

37. Hemmer W, McGlone M, Tsigelny I, Taylor SS. Role of the glycine triad in the ATP-binding site of cAMP-dependent protein kinase. J Biol Chem 1997;272:16946–54.

38. Simard JR, Getlik M, Grutter C, Schneider R, Wulfert S, Rauh D. Fluorophore labeling of the glycine-rich loop as a method of identifying inhibitors that bind to active and inactive kinase conformations. J Am Chem Soc 2010;132:4152–60.

39. Yasuda H, Park E, Yun CH, Sng NJ, Lucena-Araujo AR, Yeo WL, et al. Structural, biochemical, and clinical characterization of epidermal growth factor receptor (EGFR) exon 20 insertion mutations in lung cancer. Sci Transl Med 2013;5:216ra177.

40. Jura N, Shan Y, Cao X, Shaw DE, Kuriyan J. Structural analysis of the catalytically inactive kinase domain of the human EGF receptor 3. Proc Natl Acad Sci U S A 2009;106:21608–13.

41. Khorashad JS, Kelley TW, Szankasi P, Mason CC, Soverini S, Adrian LT, et al. BCR-ABL1 compound mutations in tyrosine kinase inhibitor-resistant CML: frequency and clonal relationships. Blood 2013;121:489–98.

42. Dai J, Kong Y, Si L, Chi Z, Cui C, Sheng X, et al. Large-scale analysis of PDGFRA mutations in melanomas and evaluation of their sensitivity to tyrosine kinase inhibitors imatinib and crenolanib. Clin Cancer Res 2013;19:6935–42.

43. Bauer S, Yu LK, Demetri GD, Fletcher JA. Heat shock protein 90 inhibition in imatinib-resistant gastrointestinal stromal tumor. Cancer Res 2006;66:9153–61.

44. Doi T, Kurokawa Y, Sawaki A, Komatsu Y, Ozaka M, Takahashi T, et al. Efficacy and safety of TAS-116, an oral inhibitor of heat shock protein 90, in patients with metastatic or unresectable gastrointestinal stromal tumour refractory to imatinib, sunitinib and regorafenib: a phase II, single-arm trial. Eur J Cancer 2019;121:29–39.

45. Hayashi Y, Bardsley MR, Toyomasu Y, Milosavljevic S, Gajdos GB, Choi KM, et al. Platelet-derived growth factor receptor-alpha regulates proliferation of gastrointestinal stromal tumor cells with mutations in KIT by stabilizing ETV1. Gastroenterology 2015;149:420–32.

46. Chi P, Chen Y, Zhang L, Guo X, Wongvipat J, Shamu T, et al. ETV1 is a lineage survival factor that cooperates with KIT in gastrointestinal stromal tumours. Nature 2010;467:849–53.

47. Ran L, Sirota I, Cao Z, Murphy D, Chen Y, Shukla S, et al. Combined inhibition of MAP kinase and KIT signaling synergistically destabilizes ETV1 and suppresses GIST tumor growth. Cancer Discov 2015;5:304–15.

48. Chi P, Qin L-X, Kelly CM, D'Angelo SP, Dickson MA, Gounder MM, et al. A phase II study of MEK162 (binimetinib [BINI]) in combination with imatinib in patients with untreated advanced gastrointestinal stromal tumor (GIST). J Clin Oncol 2020;38:11508.

49. Schwartz LH, Seymour L, Litiere S, Ford R, Gwyther S, Mandrekar S, et al. RECIST 1.1 – standardisation and disease-specific adaptations: perspectives from the RECIST Working Group. Eur J Cancer 2016;62:138–45.

50. Dressman D, Yan H, Traverso G, Kinzler KW, Vogelstein B. Transforming single DNA molecules into fluorescent magnetic particles for detection and enumeration of genetic variations. Proc Natl Acad Sci U S A 2003;100:8817–22.

51. Lanman RB, Mortimer SA, Zill OA, Sebisanovic D, Lopez R, Blau S, et al. Analytical and clinical validation of a digital sequencing panel for quantitative, highly accurate evaluation of cell-free circulating tumor DNA. PLoS One 2015;10:e0140712.

52. Auton A, Brooks LD, Durbin RM, Garrison EP, Kang HM, Korbel JO, et al. A global reference for human genetic variation. Nature 2015;526:68–74.

53. Skehan P, Storeng R, Scudiero D, Monks A, McMahon J, Vistica D, et al. New colorimetric cytotoxicity assay for anticancer-drug screening. J Natl Cancer Inst 1990;82:1107–12.

54. Duensing A, Medeiros F, McConarty B, Joseph NE, Panigrahy D, Singer S, et al. Mechanisms of oncogenic KIT signal transduction in primary gastrointestinal stromal tumors (GISTs). Oncogene 2004;23: 3999–4006.

55. Laemmli UK. Cleavage of structural proteins during the assembly of the head of bacteriophage T4. Nature 1970;227:680–5.

56. Case DA, Belfon K, Ben-Shalom IY, Brozelle SR, Cerutti DS, Cheatham TE, et al. AMBER2018. San Francisco: University of California; 2018.

57. Li P, Song LF, Merz KM Jr. Systematic parameterization of monovalent ions employing the nonbonded model. J Chem Theory Comput 2015;11:1645–57.

58. Meagher KL, Redman LT, Carlson HA. Development of polyphosphate parameters for use with the AMBER force field. J Comput Chem 2003;24:1016–25.

59. Roe DR, Cheatham TE 3rd. PTRAJ and CPPTRAJ: software for processing and analysis of molecular dynamics trajectory data. J Chem Theory Comput 2013;9:3084–95.

60. Jones G, Willett P, Glen RC, Leach AR, Taylor R. Development and validation of a genetic algorithm for flexible docking. J Mol Biol 1997;267:727–48.

61. Wang J, Wolf RM, Caldwell JW, Kollman PA, Case DA. Development and testing of a general amber force field. J Comput Chem 2004;25:1157–74.